Progress In Electromagnetics Research M, Vol. 31, 247–262, 2013

ANALYSIS AND MODELING OF POWER MOSFET RADIATION

Sofiene Saidi* **and Jaleleddine Ben Hadj Slama**

SAGE, National Engineering School of Sousse, (ENISo), University of Sousse, Technopole of Sousse, Sousse 4054, Tunisia

Abstract—This paper deals with the modeling the radiation of the power electronics component: the MOSFET. First, the magnetic near field measurements are made to characterize the radiation of the component. The MOSFET under test is referenced by IRF640 used in DC-DC converter. Second, we have applied the electromagnetic inverse method based on the measured field at 20 MHz to create a model of radiation sources of the MOSFET. The obtained results show a good agreement between the magnetic near field cartography obtained by the developed model and those measured. Finally, the developed model was used to predict the magnetic field in another distance and it was validated with measured cartography.

1. INTRODUCTION

The active components are a key element in the power electronics system. The massive use of semiconductor components with increasing switching frequencies in the power systems generates highly important voltage (dv/dt) and current (di/dt) fronts. These fast variations generate through the geometry of these systems an intense electromagnetic interference. To guarantee an electromagnetic compatibility of the systems, it is imperative to control the radiation of its various parts, especially its power systems. This requires the provision of radiation patterns of the various components of these systems.

The MOSFET is a component totally driven by its Gate-Source voltage (V_{GS}) which is characterized by two operating states: open or closed. During the switching between these two states, certain unavoidable parasitic elements appear. Several studies have examined

Received 20 May 2013, Accepted 6 July 2013, Scheduled 8 July 2013

* Corresponding author: Sofiene Saidi (saidi.sofiene@yahoo.fr).

the conducted disturbances due to the presence of the MOSFET [1] and they have developed models of circuit type for estimating these conducted disturbances [2]. It becomes interesting to examine and model the radiation of the MOSFET. The examination of the power electronics component radiation has been discussed by several studies however no one of them has proposed a radiating model to the MOSFET. The measurements of the near-field radiated by a chopper are used to find the radiation model in [3, 4]. The identified models in these studies take into account only the radiation of the switching loops because they are the most radiating elements. A model of a DC-DC converter based on a MOSFET IRLRU7821 was developed in [5] through the near-field measurements. This model was created with the ICEM technique (IC emission) to predict the near-field with an accuracy of about 3 dB. The model was created through the extraction of the radiation inductances of the MOSFET by a visual analysis of the near-field cartography. These inductances were inserted into the IC-EMC software to estimate the near-field radiated by the component. [6] examined the radiation of a MOSFET connected to a resistive load for different duty cycles, different frequencies, various power supply voltages, and various currents. In this study, several magnetic near-field measurements are performed above the MOSFET without modeling the radiation of this component.

The interconnection inside the semiconductor is made through the bounding wire. To evaluate the radiation of the bounding wire used in power electronics modules, [7] used the analytical equation of a circular inductor to estimate the electromagnetic field radiated the bounding wire inside the component package.

In this paper, we focus on the characterization and modeling of the radiation of a MOSFET. Firstly, we present the results of the magnetic near-field measurements above the MOSFET used in a DC-DC converter. The measurements are performed in the time domain in order to cover a range of emission frequencies. Secondly, we propose a model for radiation sources of the MOSFET through the electromagnetic inverse method using the measured near-field cartography. Finally, an experimental validation is performed to see the ability of the model identified to reproduce the radiation of the MOSFET

2. DESCRIPTION OF THE NEAR FIELD TEST BENCH

The circuit characterization of the radiation of the MOSFET represents an elementary switching cell consisting of two controlled switches, which are the MOSFET and the freewheeling diode (Figure 1). This

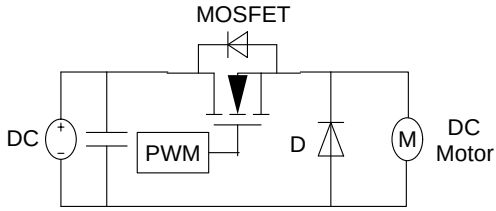

Figure 1. The switch cell based on the MOSFET.

basic representation is sufficient to consider the disturbances generated by the different types of power supplies.

The voltage and current oscillations during the opening and closing of the MOSFET appear. These oscillations generate conducted and radiated disturbances. To measure the magnetic near-field radiated by the MOSFET, we have used a time domain test bench. A near field measurement test bench is a tool to measure the electric and magnetic components field radiated by the electric system. Most of the test benches are frequency type. To measure the desired cartography, the near field test bench is equipped by an automated positioning system and a measurement chain based on spectrum analyzer (Figure 2).

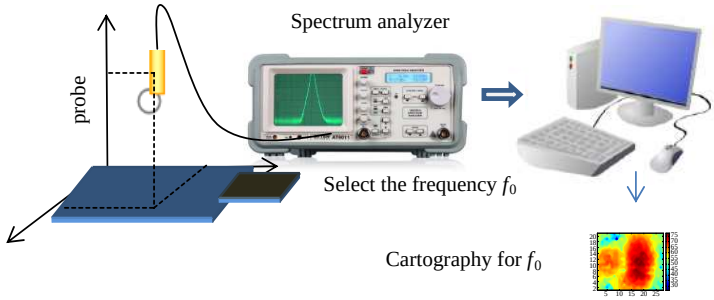

Figure 2. The near-field test bench in frequency domain.

In our application, the measurement of the radiation generated by power electronics systems is made for different radiation frequencies. We have chosen a near-field measurement test bench of a temporal type. First, this test bench allows us to analyze the radiated disturbances at each moment such as during the Turn ON and Turn OFF of power electronics switches. Second, a frequency analysis, after computing the Fast Fourier Transform (FFT) of the temporal measurements, is made to extract the near-field cartography for each

radiation frequency. Contrary to the frequency test bench, the temporal test bench requires an oscilloscope with a high precision (Figure 3).

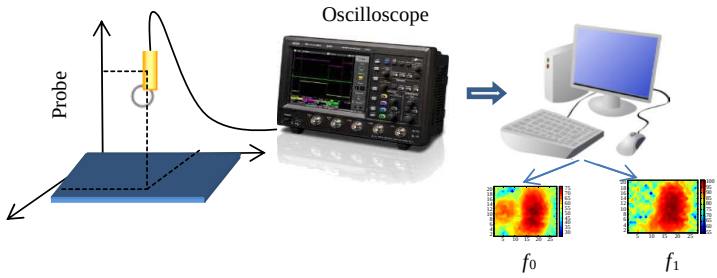

Figure 3. The near-field test bench in time domain.

The magnitude of the magnetic field is calculated in the center of the probe using Equation (1)

$$h(f) = V/2(2 \cdot \pi \cdot \mu_0 \cdot f \cdot S) \tag{1}$$

where V is the component at the frequency f of the FFT of the voltage measured at the terminals of the probe, $\mu_0 = 4 * \pi * 10^{-7}$ the vacuum permeability, $S = \pi * r^2$ the probe surface, and f the frequency of the radiated signal.

3. MEASUREMENT OF THE NEAR FIELD RADIATED BY THE MOSFET

Our study is performed using a buck converter based on a MOSFET supplied with a 30 V voltage with a duty cycle equal to 0.7, which supplies a current around 0.5 A. The switching frequency is equal to 50 kHz. The buck converter feeds a DC motor. In order to isolate the radiation of the MOSFET from the circuit chopper, we have connected the MOSFET through a twisted wire and we have moved away from the chopper circuit. When the MOSFET switches the Turn ON to Turn OFF state each 0.2 µs, a strong magnetic field is generated. To measure the temporal magnetic field, we have used an oscilloscope with a sample number of 10 GS/s. The measuring surface is 20×20 mm dimension (Figure 4), which is constituted by 400 measurement points (the measurement step = 1 mm).

Figure 5 shows the voltage measured at the terminals of the magnetic probe at a height equal to 5 mm at a point which is located above the MOSFET.

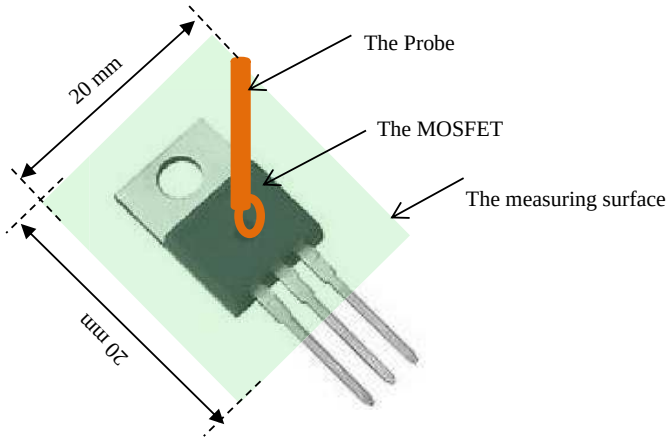

Figure 4. The MOSFET under test.

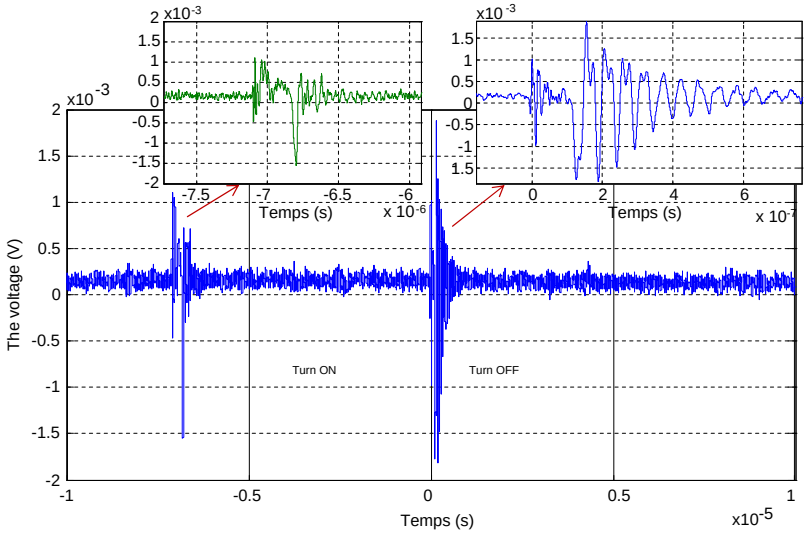

Figure 5. The measured voltage at the terminals of the probe.

From the measured magnetic field, we note the existence of switching transients on closing and opening the MOSFET. These disturbances are generated by the current variations di/dt in the switching loop. In order to examine the disturbances that propagate through the MOSFET well, we present the spectrum of the radiated magnetic field H_z. We compare in Figure 6 the specters during the

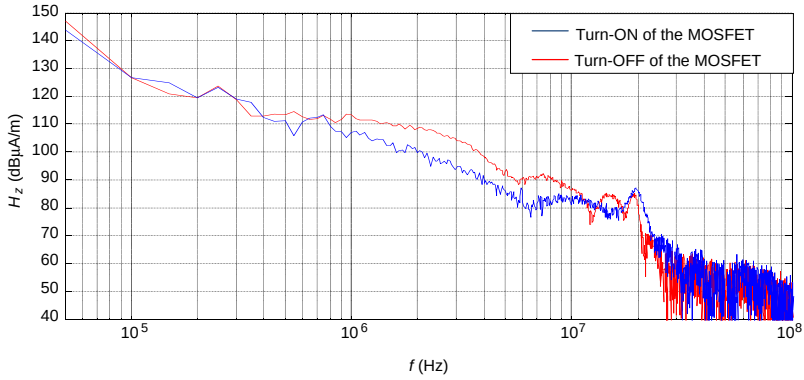

Figure 6. The spectrum of the magnetic field radiated by the MOSFET; the Turn-OFF (blue) and Turn-ON (red) of the MOSFET.

closing and opening of the MOSFET. This allows us to identify the harmonics in both switching phases.

From the frequency analysis of the two switching phases, we can identify, in low frequencies, the switching frequency and its multiples. At high frequencies, we see the appearance of several harmonics for various frequencies from 2.35 MHz to 42 MHz. We present in Table 1 the frequencies that occur during the closing and opening of the MOSFET. We note that there are some frequencies that appear only at the opening of the MOSFET; other frequencies appear only during the closing the MOSFET; and there are frequencies that appear during both the closing and the opening of the MOSFET.

Table 1. The harmonics appearing during the closing and opening of the mosfet.

frequency	Turn-OFF	Turn-ON
2.35 MHz	102 dBμA/m	
7.4 MHz	91.5 dBμA/m	
10.9 MHz		82 dBμA/m
15.4 MHz	85 dBμA/m	
19.6 MHz	86 dBμA/m	86 dBμA/m
42 MHZ	63 dBμA/m	58 dBμA/m

We note that the frequencies that appear when opening the MOSFET are more numerous than when closing. The resonances are certainly due to the current recovery of the internal diode of the

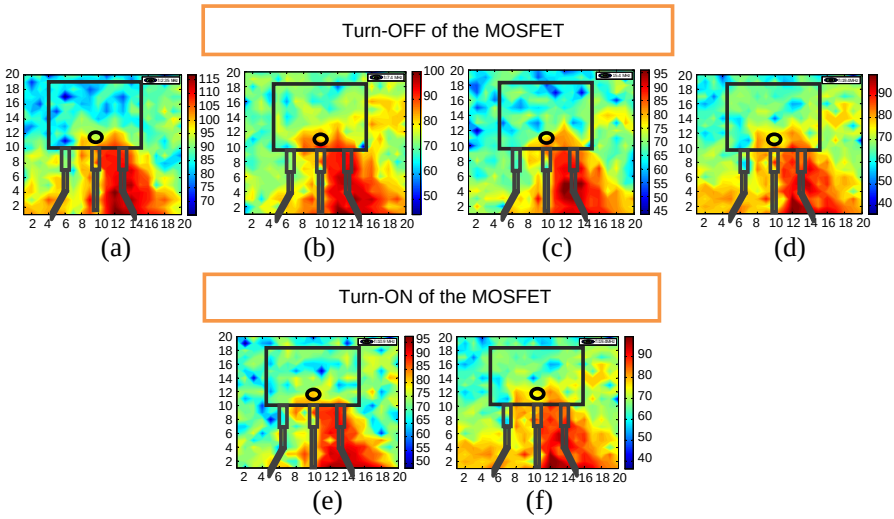

Figure 7. H_z magnetic near-field cartography. (a) $f = 2.35\,\text{MHz}$. (b) $f = 7.4\,\text{MHz}$. (c) $f = 15.4\,\text{MHz}$. (d) $f = 19.6\,\text{MHz}$. (e) $f = 10.9\,\text{MHz}$. (f) $f = 20\,\text{MHz}$.

MOSFET. We present in Figure 7 the cartographies of the H_z magnetic field measured for different frequencies.

From the H_z cartographies we can locate radiation sources at the MOSFET. We note that the area of the maximum field is located above the drain and source legs. This field is radiated by the current passing along the motor, through the drain and into the source. In fact, the control current I_{GS} which flows from the gate to the source has a low value (Figure 8).

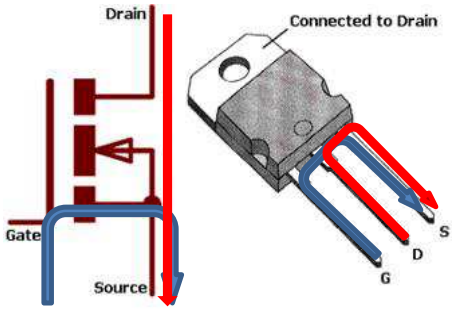

Figure 8. The current in the MOSFET.

We note that the main radiation sources are at the legs of the MOSFET. These legs behave as current loops. In order to analyze the influence of the internal part of the MOSFET in better way and eliminate the radiation of the legs, we have folded the legs of the MOSFET, as shown in Figure 9. Then we have remade the near-field measurements.

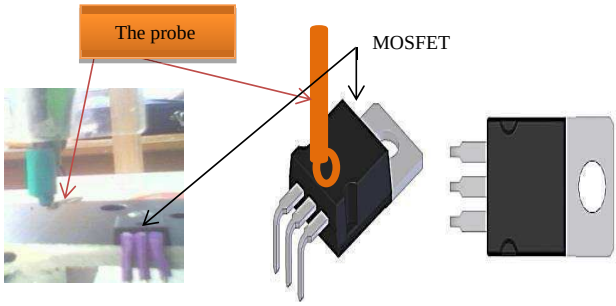

Figure 9. Characterization of the MOSFET package radiation.

We present in Figure 10 H_z the magnetic field spectrum radiated above the MOSFET at a height equal to 3 mm at the Turn ON and Turn OFF of the MOSFET.

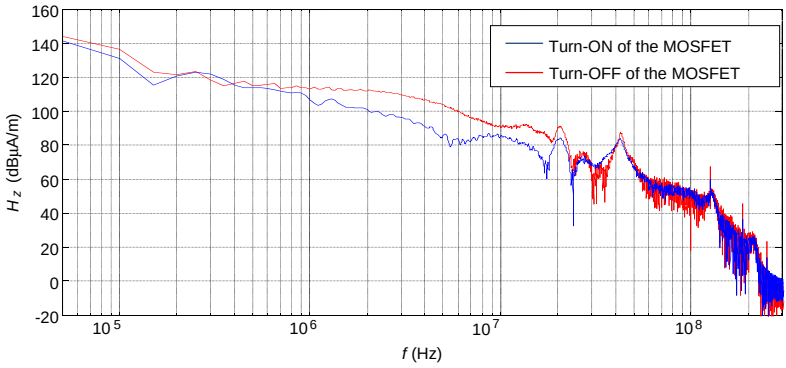

Figure 10. Spectrum of the H_z magnetic field radiated by the MOSFET.

We note from these spectra that there are five main frequencies (Table 2).

We present in Figure 11, the measured component H_z above the MOSFET for each radiation frequency.

Table 2. The harmonics appearing during the closing and opening of the MOSFET.

Frequency	TURN-OFF	TURN-ON
2.35 MHz	117 dBμA/m	
10.9 MHz		87 dBμA/m
15.4 MHz	92 dBμA/m	
20 MHz	90 dBμA/m	83 dBμA/m
42 MHZ	87 dBμA/m	83 dBμA/m

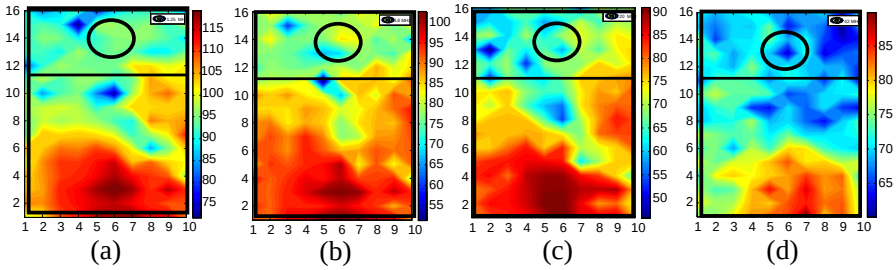

Figure 11. The cartographies of the magnetic field (H_z (dBμA/m)). (a) 2.35 MHz. (b) 10.9 MHz. (c) 20 MHz. (d) 42 MHz.

After the partial elimination of the radiation of the MOSFET legs, we note that the mapping of the magnetic field has approximately the same shape for 2.35 MHz, 10.9 MHz and 20 MHz frequencies.

We want to in the next section to identify the radiation sources of this component using the electromagnetic inverse method.

4. RADIATION MODELING OF THE MOSFET

After determining the radiation frequencies, we apply the electromagnetic inverse method for creating a radiation model of the MOSFET. This model allows us to predict the radiation of our power component (Figure 12). Modeling is to find an equivalent source from the measured magnetic field cartography using the electromagnetic inverse method based on Genetic Algorithms (GA) [8–10].

The proposed model to predict the emission of the MOSFET is based on a network of elementary electromagnetic dipoles. An elementary magnetic or electric radiating dipole is characterized by a set of parameters. That is why, The dipole can be represented by a *di* vector which includes all the parameters $d_i = (T_d,\ M_d,\ X_d,\ Y_d,$

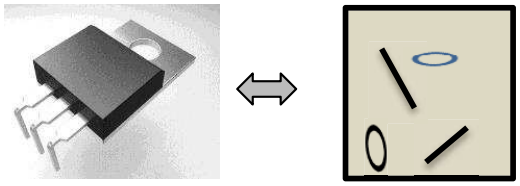

Figure 12. The model.

Z_d, θ, φ). Where T_d is the type of dipole (magnetic or electric), M_d is the magnetic moment, (X_d, Y_d, Z_d) is the dipole position and (θ, φ) is the dipole orientation. The magnetic field H_z radiated by the two elementary dipoles is described with the analytical Equations (2) and (3) [11].

For the electric dipole:

$$H_Z = \frac{j \cdot k \cdot Md}{4 \cdot \pi \cdot R} \cdot \psi(R) \cdot \left(1 + \frac{1}{j \cdot k \cdot R}\right) \cdot \begin{pmatrix} \sin(\theta\cdot) \sin(\varphi) \cdot (Y_{de} - Y_0) \\ -\sin(\theta) \cos(\varphi) \cdot (X_{de} - X_0) \end{pmatrix} \quad (2)$$

and for the magnetic dipole:

$$H_Z = -\frac{k^2}{4} \psi(R) \cdot Md \cdot \begin{bmatrix} \left(\left(1 + \frac{1}{j \cdot k \cdot R} + \frac{1}{(j \cdot k \cdot R)^2}\right) \cdot \cos(\theta)\right) \\ - \left(\left(1 + \frac{3}{j \cdot k \cdot R} + \frac{3}{(j \cdot kR)^2}\right) \cdot \frac{1}{R^2} \cdot (Z_{de} - Z_0)\right) \\ \cdot \begin{pmatrix} \cos(\theta)(Z_{de} - Z_0) \\ +\sin(\theta)\cos(\varphi)(Y_{de} - Y_0) \\ +\sin(\theta)\sin(\varphi) \cdot (X_{de} - X_0) \end{pmatrix} \end{bmatrix} \quad (3)$$

where $\psi(R)$ is the Green function, $k = \omega \cdot \sqrt{\varepsilon \cdot \mu}$ and $R = \sqrt{(X_{de} - X_0)^2 + (Y_{de} - Y_0)^2 + (Z_{de} - Z_0)^2}$: the distance between the observation point and the dipole.

The creation of the model is done through the application of the electromagnetic inverse method. First, the magnetic near-field cartography is measured at a height h which is very inferior to $\frac{\lambda}{2\pi}$ (where λ is the wavelength). Secondly, from the measured cartography, an optimization algorithm proceeds to search for optimum parameters of dipoles (magnetic moments, positions and orientations) that will give a calculated field which is closer to the measured near-field. Thirdly, identified parameters of dipoles are used to estimate the electromagnetic field at any points in the space of the studied system. The procedure for this method is described in Figure 13.

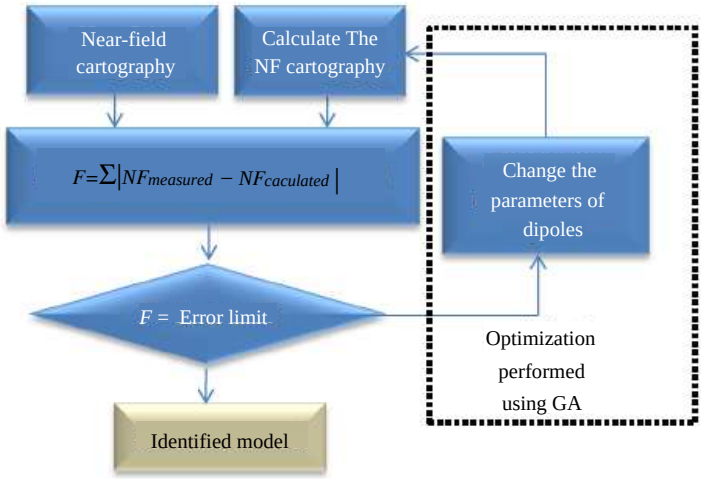

Figure 13. The electromagnetic inverse method.

To accelerate the convergence of the electromagnetic inverse method based on the GA, we refer to [12] for the choice of the GA optimal parameters (Table 3).

Table 3. The optimal parameters of the AG.

Fitness	$\sum_{i=0}^{n} \frac{\lvert H_z\_\text{réf} - H_z\_\text{calcul}\rvert}{H_z\_\text{réf}}$
Population size (Np)	20x Number of parameters $< Np <$ 30x Number of parameters
Selection function	Roulette
Crossover rate	between 0.6 and 0.8

To create a radiation model for our component, we have used the magnetic H_z field cartography at a frequency of 20 MHz. The electromagnetic inverse method is applied to search for a magnetic dipole. The identification results give us the results presented in Table 4.

Figure 14 shows the correct position of the magnetic dipole identified at the MOSFET.

Figure 15 shows the measured magnetic H_z field cartography and the one estimated with the electromagnetic inverse method. A reasonable agreement between the two cartographies is observed.

Table 4. Parameters of the identified dipole.

Excitation (A/m^2)	Magnetic moment: M_d	3.11 10^{-8}
Position of the dipole (mm)	$X_d/Y_d/Z_d$	$5.57/2.2/-1.24$
Orientation of the dipole (°)	θ/φ	$-35.46°/\ 111.8°$

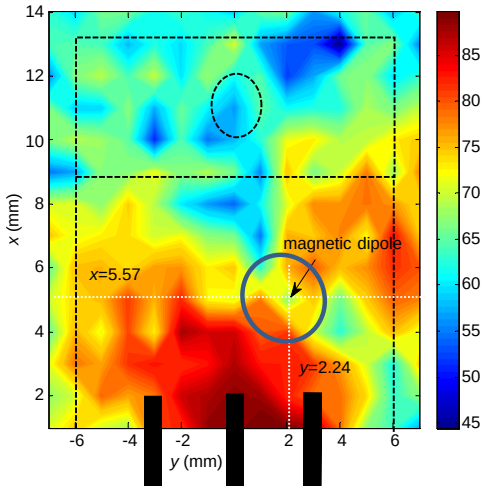

Figure 14. Position of the identified dipole.

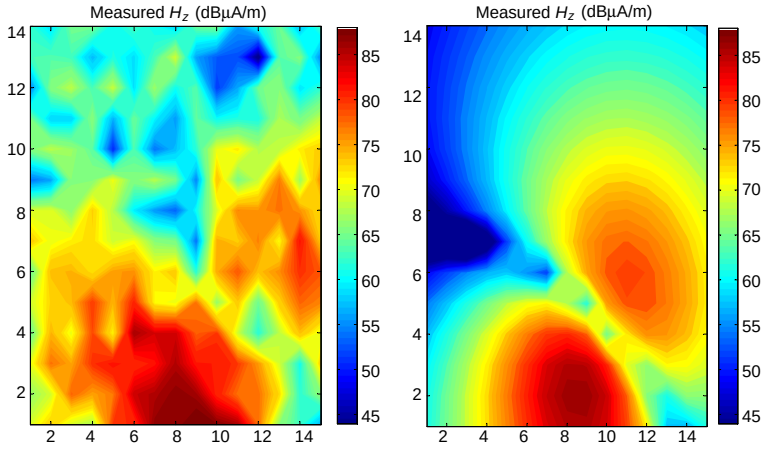

Figure 15. Measured and estimated magnetic field.

5. VALIDATION OF THE MODEL

To better validate our model, it is necessary to consider the radiation on other sides of the MOSFET. To do this, we measure the H_z magnetic field in another plane (XY) to compare with that calculated from the model found previously. The model validation is made at a frequency of 20 MHz and a height measurement equal to 2 mm (Figure 16).

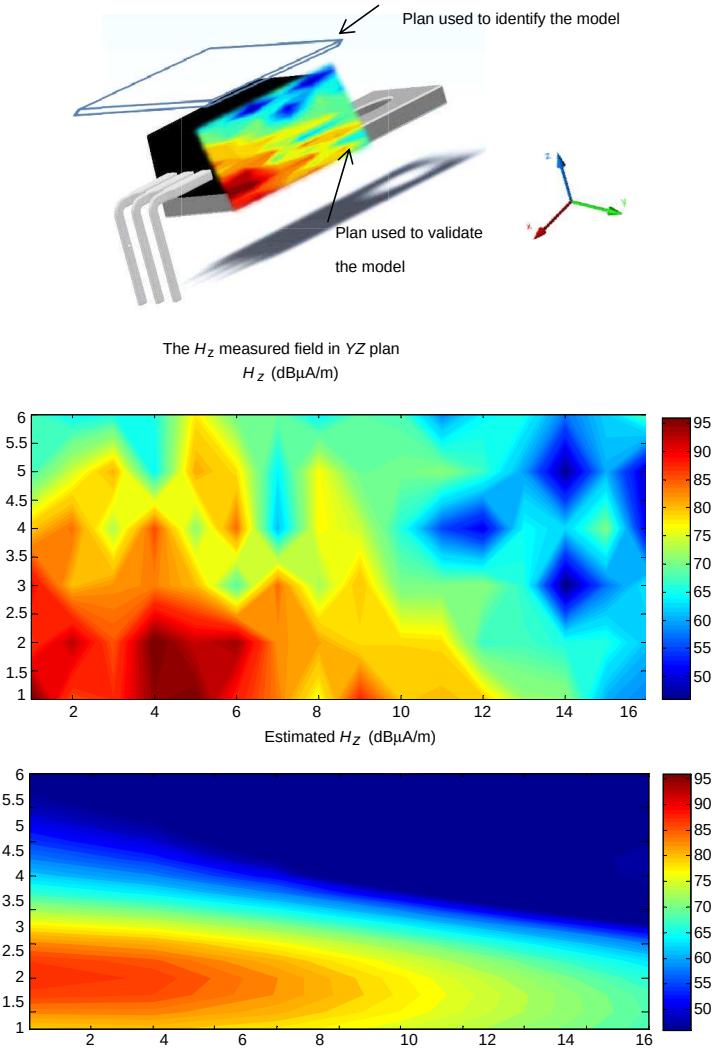

Figure 16. Measured and reconstructed H_z near-field in YZ plan.

According to previous results, the reconstructed magnetic field with the model shows a good agreement with the measured magnetic field. These results confirm the existence of an equivalent current loop. This current loop corresponds to the current of the drain to the source through the MOSFET chip.

By analyzing the bonding wire of the MOSFET IRF640, we find a current loop oriented along the z axis, as shown in Figure 17.

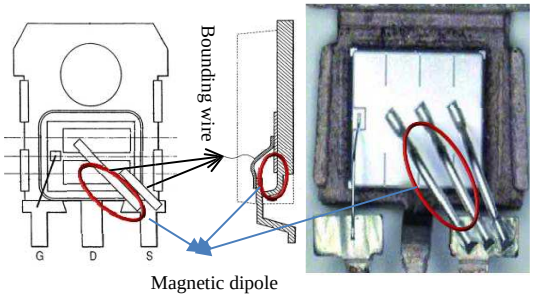

Figure 17. The internal structure of a MOSFET IRF640.

The analysis of the internal structure of the MOSFET confirms the model found by the electromagnetic inverse method. Indeed, both the I_{DS} current that passing along the MOSFET's drain to its source through the bonding wire and the MOSFET chip form a current loop equivalent to the magnetic dipole found by the inverse method. This current loop creates a strong magnetic field that depends on the I_{DS} current which traverses the MOSFET.

6. CONCLUSION

In this paper, we are interested in the study of the radiation contribution of the MOSFET power component. We have presented the identification and the modeling of the radiation of this component based on the radiated magnetic near field.

In the first section of this paper, the analysis of the measured magnetic field cartography above the MOSFET has shown that the legs of the MOSFET are the most disturbing elements.

To characterize the radiation of the MOSFET package and partially eliminate the effect of the legs, we have folded the legs of the MOSFET and we have repeated the near-field measurements.

In the second part, a radiation model of the MOSFET has been identified by using the electromagnetic inverse method and the magnetic near-field measurements. The methodology has identified a

current loop between the drain and the source of the MOSFET chip, which corresponds to the bounding wire of the component. This loop current generates a magnetic field which depends on the I_{DS} current that traverses the MOSFET. We conclude that the contribution of the MOSFET at the radiation is limited to a single current loop that corresponds to the shape of the bounding wire. In perspective, we propose to generalize this result to other types of transistors (MOSFET and IGBT).

REFERENCES

1. Ben Hadj Slama, J. and M. Tlig, "Effect of the MOSFET choice on conducted EMI in power converter circuits," *IEEE Conference on Melecon*, 610–613, Tunisia, Mar. 24–25, 2012.
2. Nicolae, P. and M. Voinea, "Modeling and simulation of electromagnetic conducted emissions from buck converter with resistive load," *International Conference on Applied and Theoretical Electricity (ICATE)*, 1–4, Oct. 25–27, 2012.
3. Beghou, L., B. Liu, L. Pichon, and F. Costa, "Synthesis of equivalent 3-D models from near field measurements application to the EMC of power printed circuits boards," *IEEE Transactions Of Magnetic*, Vol. 45, No. 3, 1650–1653, Mar. 2009.
4. Ben Hadj Slama, J. and S. Saidi, "Coupling the electromagnetic inverse problem based on genetic algorithms with moment's method for EMC of circuits," *15th IEEE Mediterranean Electrotechnical Conference, MELECON 2010*, 709–714, Malta, Italy, Apr. 2010.
5. Akue Boulingui, S. and S. Baffreau, "Near field scan method used to evaluate the parasitic emission of embedded power electronic device," *IEEE Workshop EMC*, Rouen, France, Oct. 2007.
6. Manjombe, Y. T., Y. Azzouz, D. Baudry, B. Ravelo, and M. E. H. Benbouzid, "Experimental investigation on the power electronic transistor parameters influence to the near-field radiation for the EMC applications," *Progress In Electromagnetics Research M*, Vol. 21, 189–209, 2011.
7. Gautier, C., A. Guena, and F. Costa, "Modélisation des fils de bonding utilisés en électronique de puissance," *CEM06*, Saint-Malo, France, Apr. 4–6, 2006.
8. Sijher, T. S. and A. A. Kishk, "Antenna modeling by infinitesimal dipoles using genetic algorithms," *Progress In Electromagnetics Research*, Vol. 52, 225–254, 2005.
9. Baudry, D., A. Louis, and B. Mazari, "Characterization of

the open-ended coaxial probe used for near-field measurements in EMC applications," *Progress In Electromagnetics Research*, Vol. 60, 311–333, 2006.

10. Liu, B., L. Beghou, L. Pichon, and F. Costa, "Adaptive genetic algorithm based source identification with near-field scanning method," *Progress In Electromagnetics Research B*, Vol. 9, 215–230, 2008.
11. Saidi, S. and J. Ben Hadj Slama, "Improving convergence time of the electromagnetic inverse method based on genetic algorithm using the PZMI and neural network," *Progress In Electromagnetics Research B*, Vol. 51, 389–406, 2013.
12. Saidi, S. and J. Ben Hadj Slama, "Effect of genetic algorithm parameters on convergence the electromagnetic inverse method," *International Multi-Conference on Systems, Signals & Devices, SSD2011*, 1–5, Sousse, Tunisia, Mar. 22–25, 2011.